

# High-Dimensional Inference for Unidentifiable Signals with False Negative Control <sup>\*</sup>

X. Jessie Jeng and Yifei Hu

Department of Statistics, North Carolina State University

June 6, 2022

## Abstract

False negative errors are of major concern in applications where missing a high proportion of true signals may cause serious consequences. False negative control, however, raises a bottleneck challenge in high-dimensional inference when signals are not identifiable at individual levels. We develop a new analytic framework to regulate false negative errors under measures tailored towards modern applications with high-dimensional data. A new method is proposed in realistic settings with arbitrary covariance dependence between variables. We explicate the joint effects of covariance dependence and signal sparsity on the new method and interpret the results using a phase diagram. It shows that signals that are not individually identifiable can be effectively retained by the proposed method without incurring excessive false positives. Simulation studies are conducted to compare the new method with several existing methods. The new method outperforms the others in adapting to a user-specified false negative control level. We apply the new method to analyze an fMRI dataset to locate voxels that are functionally relevant to saccadic eye movements. The new method exhibits a nice balance in retaining signal voxels and avoiding excessive noise voxels.

---

<sup>\*</sup>Address for correspondence: X. Jessie Jeng, Department of Statistics, North Carolina State University, SAS Hall, 2311 Stinson Dr., Raleigh, NC 27695-8203, USA. E-mail: xjeng@ncsu.edu.

*Keywords:* False negative proportion; Signal proportion estimation; Sparse signal; Unnecessary false positives

## 1 Introduction

False negative errors are of major concern in applications where missing true signals may cause serious consequences. For example, failures to detect active cases of highly contagious diseases may cause delayed treatment and large-scale epidemic spreading. More examples in medical, psychological, economic, and legal studies can be found in [Petticrew et al. \(2000\)](#). In modern applications with high-dimensional data, false negative control is a pressing challenge as finding true signals are often as difficult as finding needles in a haystack.

In the past decade, significant contributions have been made towards two foundational challenges in high-dimensional sparse inference. One is the detection of mixture models, which addresses the problem of “detecting” the existence of sparse signals without specifying their exact locations. The second is the identification of sparse signals, which considers the problem of “identifying” signals at individual levels. Figure 1 modified from [Donoho and Jin \(2015\)](#) illustrates the theoretical demarcation on the difficulty levels of these two problems in the setting where all variables are independent and signal variables are relatively sparse compared to the number of noise variables. Given a sparsity level, signal intensity needs to be large enough (above the undetectable region) for the signals to be detectable by a global testing procedure. For the signals to be identifiable at individual levels with multiple testing, signal intensity needs to be even larger (entering the identifiable region). It can be seen that signals in the middle region of Figure 1 can only be detected for their existence by global testing but are not identifiable at individual levels using multiple testing. Such signals commonly exist in high-dimensional data analysis and play vital roles in modern applications. Providing the capacity for retaining such signals can alleviate critical issues such as missing important signals in underpowered studies and lack of replicability across multiple samples. Despite its importance, how to effectively retain detectable yet unidentifiable signals raises a bottleneck challenge. New developments are needed to expand

the frontier of high-dimensional sparse inference and bridge the methodological gap.

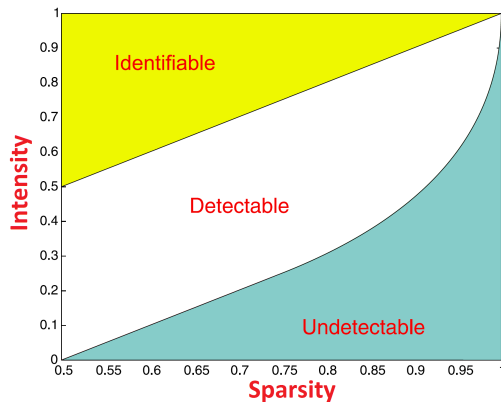


Figure 1: Phase diagram for signal detection and identification under independence. Signals in the middle region are only detectable for their existence but not identifiable at individual levels.

In this paper, we propose a novel analytic framework to regulate false negative errors under measures tailored towards modern applications with high-dimensional data. More specifically, the method controls the false negative proportion (FNP = number of false negatives/number of alternative cases) at a user-specified level and, at the same time, regulates the amount of unnecessary false positives to achieve the FNP level. We have found that, in real data analyses, researchers often have different tolerance levels for false negative errors depending on their scientific inquiries. Our procedure estimates and controls FNP at a user-specified level under conditions weak enough to allow for unidentifiable signals. Moreover, its adaptivity to a given FNP level, such as 0.1, allows the method to exclude a certain amount of the weakest signals to reduce possibly a large number of false positives.

The new method is developed in the realistic setting with arbitrary covariance dependence between variables. We propose to calibrate the overall dependence strength through a parameter whose scale is compatible with the existing parameter space in high-dimensional sparse inference. Utilizing the new calibration, we are able to explicate the joint effect of covariance dependence and signal sparsity on the new method and interpret the results using a new phase diagram, which extends the phase diagram in Figure 1 to include dependence effect. Our theoretical findings are supported in simulation examples where the data are generated under various dependence structures.

Extensive simulation studies are conducted to compare the new method with existing methods in both one-dimensional and two-dimensional examples. The new method outperforms the others in adapting to a user-specified FNP control level. We apply the new method to analyze fMRI data from the saccade experiment in the Individual Brain Charting project (Pinho et al., 2018). Compared to the other methods, results of the new method exhibit a nice balance in identifying brain regions that are functionally relevant to saccadic eye movement and avoiding the scattered or isolated voxels that are not functionally relevant to saccades.

The rest of the paper is organized as follows. Section 2 introduces the new method and justify its FNP control property in theory. Section 3 provides several illustrative examples under different dependence structures. The proposed method with the estimated number of signals is studied in Section 4, and additional simulation examples are presented in Section 5. Section 6 applies the new method to fMRI data analysis. Section 7 provides conclusion and further discussion. All the technical proofs are presented in the Appendix.

## 2 Method and Theory

We consider a model with continuous null distribution  $F_0$ . Suppose that the test statistics

$$X_j \sim F_0 \cdot 1\{j \in I_0\} + F_j \cdot 1\{j \in I_1\}, \quad j = 1, \dots, p,$$

where  $I_0$  is the set of indices for noise variables,  $I_1$  is the set of indices for signal variables, and  $F_j$  are the signal distributions. All  $I_0$ ,  $I_1$ , and  $F_j$  are unknown. One can perform inverse normal transformation as  $Z_j = \Phi^{-1}(F_0(X_j))$ , where  $\Phi^{-1}$  is the inverse of the standard normal cumulative distribution. Then, we have

$$Z_j \sim \Phi \cdot 1\{j \in I_0\} + G_j \cdot 1\{j \in I_1\}, \quad j = 1, \dots, p, \quad (1)$$

where  $G_j$  are the unknown signal distributions after the transformation. For presentation simplicity, we assume that  $G_j(t) < \Phi(t)$  for all  $t \in \mathbb{R}$ . i.e., signal variables tend to show

larger values than noise variables. This assumption can be easily generalized to signals with two-sided effects.

Consider a selection rule with threshold  $t$ . Define the numbers of selected cases, false positives, and false negatives as

$$R(t) = \sum_{j=1}^p 1_{\{z_j > t\}}, \quad FP(t) = \sum_{j \in I_0} 1_{\{z_j > t\}}, \quad FN(t) = \sum_{j \in I_1} 1_{\{z_j \leq t\}}.$$

Note that  $R(t)$  can be directly observed from the data.  $FN(t)$  and  $FP(t)$  are unknown because  $I_0$  and  $I_1$  are unknown. A generalization to two-sided signal effects can be accommodated by replacing  $z_j$  with  $|z_j|$  and only allowing  $t > 0$ . Next, define FNP with respect to  $t$  as

$$FNP(t) = FN(t)/s, \quad (2)$$

where  $s$  denotes the number of signal variables, i.e.  $s = |I_1|$ .  $FNP(t)$  may be regarded as the empirical type II error that is non-decreasing with respect to  $t$ .

## 2.1 Estimation of False Negative Proportion

The new method is based on consistent estimation of FNP. By the fact that  $s = FN(t) + TP(t)$  and  $R(t) = FP(t) + TP(t)$ , we have

$$FNP(t) = FN(t)/s = 1 - (R(t) - FP(t))/s, \quad (3)$$

where  $R(t)$  is directly observable from the data. Because the noise distribution of  $Z_j$  is  $N(0, 1)$  and there are  $p - s$  noise variables,  $FP(t)$  can be approximated by its mean value  $E(FP(t)) = (p - s)\bar{\Phi}(t)$ , where  $\bar{\Phi}(t) = 1 - \Phi(t)$ . For illustration purpose, we first assume that the true value of  $s$  is known and construct an estimator for  $FNP(t)$  as

$$\widehat{FNP}(t) = \max\{1 - R(t)/s + (p - s)\bar{\Phi}(t)/s, 0\}. \quad (4)$$

$\widehat{\text{FNP}}(t)$  with an estimated  $s$  will be discussed in [Section 4](#). Note that  $\widehat{\text{FNP}}(t)$  is not the mean value of  $\text{FNP}(t)$ , and its construction does not require information of the signal distribution  $G$ . If two-sided signal effects are under consideration, we can simply modify  $\widehat{\text{FNP}}(t)$  by replacing  $(p - s)$  with  $2(p - s)$ .

Next, we study the estimation consistency of  $\widehat{\text{FNP}}(t)$ . It is a challenging problem because the denominator  $s$  is often much smaller than  $p$ , which can explode the scale of the ratio and hence the approximation error. This causes fundamental differences in analyzing the consistency of FNP estimation and FDP estimation. Specifically, we adopt the existing calibration in sparse inference for  $s$  as

$$s = s_p = p^{1-\gamma}, \quad \gamma \in (0, 1]. \quad (5)$$

It can be seen that when  $\gamma > 0$ ,  $s$  is of a smaller order than the data dimension  $p$ , and when  $\gamma = 1$ , the number of signals does not change with  $p$ .

We are particularly interested in FNP estimation under general covariance dependence. To this end, we assume that

$$(Z_1, \dots, Z_p) \sim N_p(\mu, \Sigma), \quad (6)$$

where  $\mu$  is a  $p$ -dimensional vector with  $\mu_j = A_j \cdot 1\{j \in I_1\}$ ,  $A_j > 0$ , and  $\Sigma$  is an arbitrary correlation matrix. Define

$$\bar{\rho} = \|\Sigma\|_1/p^2,$$

where  $\|\Sigma\|_1 = \sum_{ij} |\sigma_{ij}|$ . In high-dimensional data analysis with large  $p$ ,  $\bar{\rho}$  is often very close to zero because not every variable is correlated to all the other variables. For example,  $\bar{\rho}$  of the  $\Sigma_{p \times p}$  from an autoregressive model has the order of  $p^{-1}$ . In order to calibrate the dependence effect in a scale that is compatible with the existing parameter space in sparse inference, we introduce parameter  $\eta$  through the following re-parameterization:

$$\bar{\rho} = \bar{\rho}_p = p^{-\eta}, \quad \eta \in [0, 1]. \quad (7)$$

The parameter  $\eta$  is in a constant scale and decreases with  $\bar{\rho}$ .  $\eta = 0$  corresponds to the

extremely dependent case where every variable is correlated to all the other variables, and, at the opposite end,  $\eta = 1$  corresponds to the independent case.

With  $\gamma$  and  $\eta$  representing signal sparsity and overall strength of covariance dependence, respectively, we discover a lower bound of  $t$  for the estimation consistency of  $\widehat{FNP}(t)$ , which is presented as follows:

$$\mu_{min} = \min\{\mu_1, \mu_2\}, \quad (8)$$

where

$$\mu_1 = \sqrt{2\gamma \log p} \quad \text{and} \quad \mu_2 = \sqrt{(4\gamma - 2\eta)_+ \log p + 4 \log \log p}.$$

The lower bound  $\mu_{min}$  takes the value of either  $\mu_1$  or  $\mu_2$ , depending on whichever is lower. It can be seen that  $\mu_2 < \mu_1$  when  $\eta$  is large enough or, in other words, when covariance dependence is weak enough. As dependence gets stronger and  $\eta$  gets smaller,  $\mu_1 < \mu_2$  and the lower bound equals to  $\mu_1$  and stops to change with  $\eta$ . The term  $\log \log p$  is a technical term for asymptotic analysis. We have the following theorem to summarize the estimation result.

**Theorem 2.1.** *Consider model (6). When  $t \geq \mu_{min}$ , where  $\mu_{min}$  is defined in (8),  $\widehat{FNP}(t)$  constructed in (4) consistently estimates  $FNP(t)$ , i.e.*

$$|\widehat{FNP}(t) - FNP(t)| = o_P(1). \quad (9)$$

One can see that the consistency of  $\widehat{FNP}(t)$  is achieved with  $t$  increasing with  $p$  in a  $\sqrt{\log p}$  scale. This is substantially different from the analysis in FDR studies, where the consistency of FDR/FDP estimation is studied with  $t$  as a constant. The result explicates the interesting relationship between covariance dependence ( $\eta$ ) and signal sparsity ( $\gamma$ ) in determining the consistency of  $\widehat{FNP}(t)$  for varying  $t$ .

## 2.2 Controlling FNP at a User-Specified Level

In real studies, researchers may have different tolerance levels for false negative errors. The proposed method allows a user-specified control level on FNP and efficiently selects a subset

of candidates to achieve the control level. Moreover, its adaptivity to a pre-specified low FNP level, such as 0.1, allows the method to exclude a small percent of the weakest signals to reduce possibly a large number of false positives.

Our method is constructed based on the estimator  $\widehat{FNP}$  developed in Section 2.1. Given a user-specified constant  $\beta (> 0)$ , we determine the selection threshold as

$$\hat{t}(\beta) = \sup \{t : \widehat{FNP}(t) < \beta\}, \quad (10)$$

and select all the candidates with  $z_j > \hat{t}(\beta)$ . We refer to this procedure as a dual control method. It can be seen that when all variables are ranked such that  $z_{(1)} \geq z_{(2)} \geq \dots \geq z_{(p)}$ , the dual control method selects the smallest subsets from the top whose estimated FNP is less than  $\beta$ . If two-sided signal effects are considered, all candidates with  $|z_j| > \hat{t}(\beta)$  will be selected.

The following theorem presents the dual control property of the proposed method which is to regulate both the FNP at a pre-specified  $\beta$  level and the associated false positives.

**Theorem 2.2.** *Consider model (6) and a user-specified control level  $\beta$  of FNP. Assume  $A_j - \mu_{min} \rightarrow \infty, \forall j \in I_1$ , where  $\mu_{min}$  is defined in (8), then the dual control method with threshold  $\hat{t}(\beta)$  efficiently controls the true FNP at the level of  $\beta$ , i.e.,*

$$P(FNP(\hat{t}(\beta)) \leq \beta) \rightarrow 1, \quad (11)$$

and, for any smaller set of variables associated with threshold  $\tilde{t} > \hat{t}(\beta)$ ,

$$P\{FNP(\tilde{t}) > \beta - \delta\} \rightarrow 1 \quad (12)$$

for arbitrarily small constant  $\delta > 0$ .

Theorem 2.2 shows efficiency of the dual control method in selecting the smallest subset of variables to achieve FNP control at the  $\beta$  level. In other words, the method does not incur unnecessary false positives to achieve the FNP control level. The condition on signal intensity ( $A_j$ ) specifies the joint effect of covariance dependence and signal sparsity on the

dual control method. Recall  $\mu_{min} = \min\{\mu_1, \mu_2\}$ , where  $\mu_1$  only relies on signal sparsity ( $\gamma$ ), and  $\mu_2$  replies on both signal sparsity ( $\gamma$ ) and covariance dependence ( $\eta$ ). The condition says that the difficulty of dual control increases as dependence gets stronger, but only to a certain degree that depends on the signal sparsity.

The parameterization of covariance dependence through  $\eta$  allows us to present the signal intensity condition using a phase diagram similar to [Figure 1](#). More specifically, let  $\min_{j \in I_1} A_j = \sqrt{2r \log p}$ ,  $r > 0$ . The condition on  $A_j$  in [Theorem 2.2](#) can be transformed to  $r > \min\{\gamma, 2\gamma - \eta\}$  and demonstrated in a two-dimensional phase diagram with  $\gamma$  as the x axis and  $r$  as the y axis. The lower bound  $\min\{\gamma, 2\gamma - \eta\}$  is illustrated in [Figure 2](#) by the red solid line that moves with the dependence parameter  $\eta$ . Signals in the area above the red solid line can be efficiently retained by the dual control method at a pre-specified level. Recall [Figure 1](#), which implies that under independence, signals in the region between the two dashed lines are only detectable for their existence but not identifiable at individual levels. The special case of our results under independence ( $\eta = 1$ ) shows that many of the unidentifiable signals can be efficiently retained by the new method.

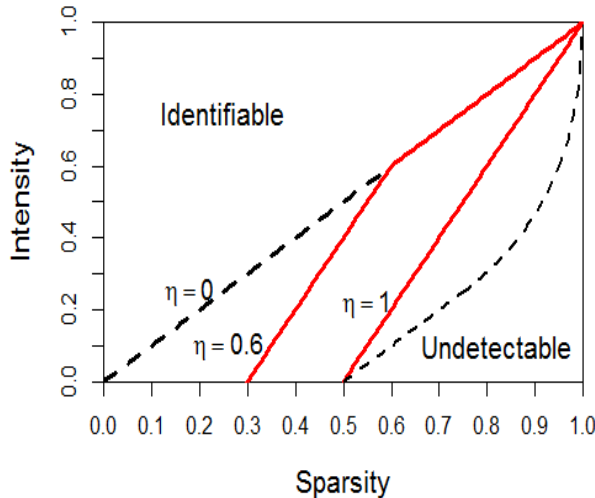


Figure 2: Dual control region under covariance dependence. Signals in the area above a solid red line can be retained by the dual control method at a pre-specified FNP level. The area increases with  $\eta$  as the dependence get weaker.

### 3 Examples

In this section, we present simulation examples with different dependence structures to illustrate the performance of the new method. We first evaluate the estimator  $\widehat{\text{FNP}}(t)$  from (4), then demonstrate finite sample results of the dual control method. These examples help understand the foundation of the new method. Additional simulation studies are provided in Section 5.

We generate a series of test statistics

$$(Z_1, \dots, Z_p)^T \sim N((\mu_1, \dots, \mu_p)^T, \Sigma), \quad (13)$$

where  $p = 2000$ ,  $\mu_j = A \cdot 1\{j \in I_1\}$ , and  $I_1$  is a set of indices randomly sampled from  $\{1, \dots, p\}$  with cardinality  $s = |I_1| = p^{1-\gamma}$ . We set  $\gamma = 0.3$ , which corresponds to  $s = 205$ , i.e. there are 205 signal variables with elevated mean values randomly located among 1795 noise variables. The signal intensity varies with  $A = 3$  and 2. . We consider three different dependence structures:

- Model 1 [Autoregressive]:  $\Sigma = (\sigma_{ij}^{(1)})$ , where  $\sigma_{ij}^{(1)} = \lambda^{|i-j|}$  for  $1 \leq i, j \leq p$ .
- Model 2 [Block dependence]:  $\Sigma = \mathbf{I}_{p/k} \otimes \mathbf{D}$ , where  $\mathbf{D}$  is a  $k \times k$  matrix with diagonal entries 1 and off-diagonal entries  $r$ .
- Model 3 [Factor model]:  $\Sigma = (\sigma_{ij}^{(3)})$ , where  $\sigma_{ij}^{(3)} = V_{ij}/\sqrt{V_{ii}V_{jj}}$  for  $1 \leq i, j \leq p$ ,  $\mathbf{V} = \tau \mathbf{h} \mathbf{h}^T + \mathbf{I}_p$  with  $\tau \in (0, 1)$  and  $\mathbf{h} \sim N(\mathbf{0}, \mathbf{I}_p)$ .

In this section, we set  $\lambda = 0.2$ ,  $k = 40$ ,  $r = 0.5$ , and  $\tau = 0.5$ , so that the dependence parameter  $\eta$  decreases from 0.95 in Model 1 to 0.57 in Model 2 to 0.23 in Model 3. Correspondingly, dependence among test statistics increases from very weak in Model 1 to moderately strong in Model 2 to very strong in Model 3.

It has been derived in Section 2.1 that  $\mu_{min}$ , as the boundary value for estimation consistency, is the minimum of  $\mu_1$  and  $\mu_2$ , where  $\mu_1$  depends on signal sparsity through  $\gamma$  and  $\mu_2$  depends on both signal sparsity and dependence through  $\gamma$  and  $\eta$ . In these examples,  $(\mu_1 = 2.14, \mu_2 = 1.69)$  for Model 1,  $(\mu_1 = 2.14, \mu_2 = 2.92)$  for Model 2, and

$(\mu_1 = 2.14, \mu_2 = 3.69)$  for Model 3. Consequently,  $\mu_{min} = 1.69$  for Model 1 but remains the same at 2.14 for Model 2 and 3. These values of  $\mu_{min}$  are illustrated as the solid vertical lines in [Figure 3](#). The dotted vertical lines represent  $\mu_1$  or  $\mu_2$  whichever is larger. The dotted curves represent the absolute difference between the estimated  $\widehat{FNP}(t)$  and the true  $FNP(t)$  from 100 replications. It can be seen that the estimation accuracy of  $\widehat{FNP}(t)$  increases with  $t$ , and the majority of the replicated differences are close to 0 after passing  $\mu_{min}$ , which support  $\mu_{min}$  as the boundary value for estimation consistency under very different dependence structures.

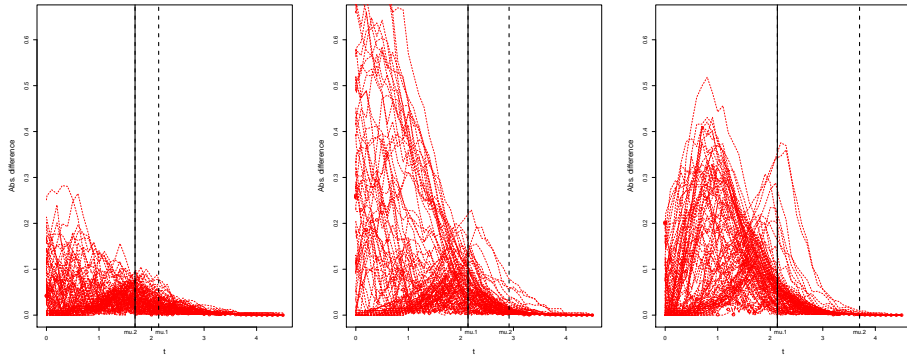


Figure 3: Estimation accuracy of  $\widehat{FNP}(t)$  based on 100 replications. Plots from left to right are generated under Model 1 - 3. The solid vertical lines represent the boundary value  $\mu_{min} = \min\{\mu_1, \mu_2\}$ . Model 1 has very weak dependence with  $\eta = 0.95$  and  $\mu_{min} = \mu_2 = 1.69$ . Model 2 has moderately strong dependence with  $\eta = 0.57$  and  $\mu_{min} = \mu_1 = 2.14$ . Model 3 has very strong dependence with  $\eta = 0.23$  and  $\mu_{min} = \mu_1 = 2.14$ .

Next, we demonstrate the finite sample performance of the dual control method, which is denoted as DCOE (acronym for Dual Control Of Errors) in [Table 1](#). We present the mean values and standard deviations of the realized FNP of DCOE with different  $\beta$  levels from 100 replications. The results of DCOE are compared with those of the classical BH-FDR procedure ([Benjamini and Hochberg, 1995](#)) with different nominal levels. For illustrative purposes, we also present the mean values of the realized false discovery proportion (FDP) of the two methods.

It can be seen that for Model 1 [Autoregressive], the mean values of FNP for DCOE with  $\beta = 0.2$  and 0.1 are fairly close to their corresponding nominal levels. Specifically, when  $A = 3$  we have 0.198 and 0.101 respectively, and when  $A = 2$ , we have 0.201 and 0.114

Table 1: Mean values and standard deviations (in brackets) of the realized FNP and FDP of the proposed DCOE method with different nominal levels and the existing BH-FDR procedure with different nominal levels.

			FNP	FDP
A=3	Autoregressive	DCOE( $\beta = 0.2$ )	<b>0.198</b> (0.023)	0.149 (0.035)
		DCOE( $\beta = 0.1$ )	<b>0.101</b> (0.037)	0.307 (0.084)
		BH-FDR( $\alpha = 0.05$ )	0.378 (0.040)	<b>0.044</b> (0.018)
		BH-FDR( $\alpha = 0.2$ )	0.166 (0.028)	<b>0.183</b> (0.028)
Block dependence		DCOE( $\beta = 0.2$ )	<b>0.170</b> (0.086)	0.259 (0.247)
		DCOE( $\beta = 0.1$ )	<b>0.089</b> (0.074)	0.444 (0.268)
		BH-FDR( $\alpha = 0.05$ )	0.387 (0.071)	<b>0.047</b> (0.036)
		BH-FDR( $\alpha = 0.2$ )	0.169 (0.049)	<b>0.180</b> (0.070)
Factor model		DCOE( $\beta = 0.2$ )	<b>0.160</b> (0.099)	0.262 (0.215)
		DCOE( $\beta = 0.1$ )	<b>0.084</b> (0.104)	0.533 (0.227)
		BH-FDR( $\alpha = 0.05$ )	0.400 (0.043)	<b>0.041</b> (0.049)
		BH-FDR( $\alpha = 0.2$ )	0.176 (0.049)	<b>0.170</b> (0.113)
A=2	Autoregressive	DCOE( $\beta = 0.2$ )	<b>0.201</b> (0.069)	0.576 (0.073)
		DCOE( $\beta = 0.1$ )	<b>0.114</b> (0.069)	0.688 (0.085)
		BH-FDR( $\alpha = 0.05$ )	0.889 (0.035)	<b>0.040</b> (0.043)
		BH-FDR( $\alpha = 0.2$ )	0.630 (0.050)	<b>0.181</b> (0.044)
Block dependence		DCOE( $\beta = 0.2$ )	<b>0.193</b> (0.132)	0.607 (0.161)
		DCOE( $\beta = 0.1$ )	<b>0.132</b> (0.116)	0.685 (0.152)
		BH-FDR( $\alpha = 0.05$ )	0.894 (0.058)	<b>0.055</b> (0.070)
		BH-FDR( $\alpha = 0.2$ )	0.647 (0.097)	<b>0.182</b> (0.093)
Factor model		DCOE( $\beta = 0.2$ )	<b>0.188</b> (0.169)	0.642 (0.107)
		DCOE( $\beta = 0.1$ )	<b>0.156</b> (0.159)	0.693 (0.098)
		BH-FDR( $\alpha = 0.05$ )	0.886 (0.088)	<b>0.032</b> (0.061)
		BH-FDR( $\alpha = 0.2$ )	0.659 (0.088)	<b>0.160</b> (0.123)

respectively.

In the more challenging cases generated by Model 2 [Block dependence] and 3 [Factor model], the boundary value  $\mu_{min}$  required for estimation consistency increases from 1.69 to 2.14; and the differences between realized FNPs of DCOE and the nominal levels increase slightly. These observations agree with the theoretical results in Sections 2.2.

For illustrative purposes, we also present the results of the classical BH-FDR procedure. The nominal levels of BH-FDR are set at  $\alpha = 0.05$  and 0.2. Table 1 shows that the mean values of the realized FDP of BH-FDR are fairly close to their corresponding nominal levels of  $\alpha$ . However, the mean values of FNP for BH-FDR are generally larger than those of

DCOE, especially when signal intensity is relatively weak. It is true that one can always increase the nominal level of BH-FDR to reduce FNP, but it is unclear by how much we should increase  $\alpha$  to achieve a target level of FNP. For example, when  $A = 3$ , BH-FDR with  $\alpha = 0.2$  has the mean values of FNP in the range of 0.166-0.176 for the three dependence models, which seem to be comparable to the FNP range of DCOE with  $\beta = 0.2$ . However, when  $A = 2$ , BH-FDR with  $\alpha = 0.2$  has much bigger mean values of FNPs in the range of 0.63 - 0.66.

These results demonstrate the fundamental differences between multiple testing procedures and the proposed dual control method as they serve for very different purposes. The proposed method aims to retain more signals with a target FNP level, for which the multiple testing methods cannot achieve. On the other hand, the new method pays the price of having a higher FDP. Additional simulation examples illustrating the efficiency of the new method compared to other false negative control methods are presented in Section 5

## 4 FNP control with estimated number of signals

Implementation of the new method requires information of the number of signals ( $s$ ) which, in real applications, is often unknown. Existing studies for the estimation of  $s$  usually assume independence among variables (Genovese and Wasserman, 2004; Meinshausen and Rice, 2006; Cai et al., 2007; Cai and Jin, 2010), and most of them are for relatively dense signals. We are interested in finding an estimator of  $s$  that works in our setting with arbitrary covariance dependence. Recent study in Jeng (2021) introduces an estimator for the signal proportion  $\pi (= s/p)$  with the form  $\hat{\pi} = \max\{\hat{\pi}_\delta, \delta \in \Delta\}$ , where  $\Delta$  is a set of functions that render the most powerful consistent estimators in a family of estimators under different dependence scenarios. More specifically, the family of estimators are defined as

$$\hat{\pi}_\delta = \sup_{t>0} \frac{R(t)/p - 2\bar{\Phi}(t) - c_{p,\delta}\delta(t)}{1 - 2\bar{\Phi}(t)}, \quad (14)$$

where  $\delta(t)$  is a strictly positive function on  $(0, \infty)$  and  $c_{p,\delta}$  is its corresponding bounding sequence. It is discovered that  $\delta(t) = [\bar{\Phi}(t)]^{1/2}$  and  $\delta(t) = \bar{\Phi}(t)$  result in powerful  $\hat{\pi}_\delta$  under

different dependence scenarios, and a new estimator is developed as

$$\hat{\pi} = \max\{\hat{\pi}_{0.5}, \hat{\pi}_1\}, \quad (15)$$

where  $\hat{\pi}_{0.5}$  denotes  $\hat{\pi}_\delta$  with  $\delta = [\bar{\Phi}(t)]^{1/2}$ , and  $\hat{\pi}_1$  denotes  $\hat{\pi}_\delta$  with  $\delta = \bar{\Phi}(t)$ . Details about the selection of  $\delta(t)$ , the construction of  $c_{p,\delta}$ , and the properties of  $\hat{\pi}_\delta$  and  $\hat{\pi}$  can be found in [Jeng \(2021\)](#).

We extend the results in [Jeng \(2021\)](#) to our setting with  $\gamma$  and  $\eta$  representing signal sparsity and overall covariance strength, respectively, so that the conditions for the consistency of  $\hat{\pi}$  and the conditions for the FNP control of our proposed method can be unified. Because the theoretical analysis in [Jeng \(2021\)](#) is conducted on a discretized version  $(\hat{\pi}_\delta^*)$  of  $\hat{\pi}_\delta$ , which is defined by replacing  $\sup_{t>0}$  in (14) with  $\max_{t \in \mathbb{T}}$ , where  $\mathbb{T} = [1, \sqrt{5 \log p}] \cap \mathbb{N}$ , we present the unified conditions for the discretized version of  $\hat{\pi}$  as well and define it as  $\hat{\pi}^* = \max\{\hat{\pi}_{0.5}^*, \hat{\pi}_1^*\}$ .

**Proposition 4.1.** *Assume the same conditions as in Theorem 2.2. Then, for any constant  $\epsilon > 0$ ,*

$$P((1 - \epsilon) < \hat{\pi}^*/\pi < 1) \rightarrow 1. \quad (16)$$

Replace  $s$  in (10) with the estimator  $\hat{s} = p \cdot \hat{\pi}^*$  and denote the selection threshold as  $\hat{t}_{\hat{s}}(\beta)$ . We have

$$P(FNP(\hat{t}_{\hat{s}}(\beta)) \leq \beta) \rightarrow 1 \quad (17)$$

and, for any threshold  $\tilde{t} > \hat{t}_{\hat{s}}(\beta)$ ,

$$P\{FNP(\tilde{t}) > \beta - \delta\} \rightarrow 1 \quad (18)$$

for arbitrarily small constant  $\delta > 0$ .

[Proposition 4.1](#) shows that the same set of conditions are sufficient for both the consistency of  $\hat{\pi}^*$  and the efficient FNP control of the proposed method implemented with  $\hat{\pi}^*$ . This result can also be interpreted by the phase diagram in [Figure 2](#), where the solid red line that moves with the dependence level  $\eta$  now indicates the required signal intensity for both

$s$  estimation and FNP control. In other words, for signals above the solid red line, although they may not be individually identifiable, we can still perform meaningful inference by not only estimating their total numbers but also effectively retaining them at a target FNP level.

Generally speaking, if we want to derive information of sparse signals from a dataset, a condition on the signal intensity is unfortunately unavoidable. When signal intensity is too low, no methods can even detect their existence (Donoho and Jin, 2004; Arias-Castro et al., 2011; Cai et al., 2011), let along the more challenging tasks of FNP estimation and control. When the condition on signal intensity does not hold, the estimator  $\hat{\pi}$  tends to underestimate because of its lower bound property (Jeng, 2021). Consequently, the dual control method implemented with  $\hat{s} = p \cdot \hat{\pi}$  tends to have a threshold higher than the ideal threshold that achieves the target level of  $\beta$ , which results in conservative variable selection with inflated FNP and correspondingly less false positives. This tendency is observed in simulation examples with low signal-to-noise ratio in Section 5.1.

We conclude the section with numerical algorithms to calculate the bounding sequence  $c_{p,\delta}$  and the proportion estimator  $\hat{\pi}$  in (14), and to select variables by the dual control method.

---

**Algorithm 1** Bounding Sequence  $c_{p,\delta}$ 


---

**Input:**  $N$  sets of  $\{w_1, \dots, w_p\}$  generated by the joint null distribution of  $\{z_1, \dots, z_p\}$

**Output:** bounding sequences  $c_{p,0.5}$  and  $c_{p,1}$

1: **for**  $a = 1, 2, \dots, N$  **do**

Rank the  $a$ -th set of  $\{w_1, \dots, w_p\}$  such that  $w_{(1)} > w_{(2)} > \dots > w_{(p)}$

Compute

$$V_{0.5,a} = \max_{1 \leq j \leq p} \frac{|j/p - \bar{\Phi}(w_{(j)})|}{\sqrt{\bar{\Phi}(w_{(j)})}} \quad \text{and} \quad V_{1,a} = \max_{1 \leq j \leq p} \frac{|j/p - \bar{\Phi}(w_{(j)})|}{\bar{\Phi}(w_{(j)})}$$

2: **end for**

3: Compute  $c_{p,0.5}$  and  $c_{p,1}$  as the  $(1 - 1/\sqrt{\log p})$ -th quantiles of the empirical distributions of  $V_{0.5,a}$  and  $V_{1,a}$ , respectively

---

Note that the computation of  $c_{p,\delta}$  requires input of statistics generated by the joint null distribution. When the joint null distribution is unknown in real applications, we often can simulate such statistics non-parametrically. For example, when  $\{z_1, \dots, z_p\}$  are a set of test statistics for associations between a set of explanatory variables and a response variable, we may randomly shuffling only the sample of the response variable to remove the potential associations and then calculate the test statistics.

---

**Algorithm 2** Signal Proportion Estimator

---

**Input:** test statistics  $\{z_1, \dots, z_p\}$  and bounding sequences  $c_{p,0.5}$  and  $c_{p,1}$

**Output:** a proportion estimate  $\hat{\pi}$

- 1: Rank the variables by their test statistics so that  $z_{(1)} > z_{(2)} > \dots > z_{(p)}$
- 2: Compute

$$\hat{\pi}_{0.5} = \max_{1 \leq j \leq p} \frac{j/p - \bar{\Phi}(z_{(j)}) - c_{p,0.5} \sqrt{\bar{\Phi}(z_{(j)})}}{1 - \bar{\Phi}(z_{(j)})} \quad \text{and} \quad \hat{\pi}_1 = \max_{1 \leq j \leq p} \frac{j/p - \bar{\Phi}(z_{(j)}) - c_{p,1} \bar{\Phi}(z_{(j)})}{1 - \bar{\Phi}(z_{(j)})}$$

- 3: Obtain  $\hat{\pi} = \max\{\hat{\pi}_{0.5}, \hat{\pi}_1\}$

---



---

**Algorithm 3** Dual Control Procedure

---

**Input:** test statistics  $z_1, \dots, z_p$ , a user-specified  $\beta$ , and a proportion estimate  $\hat{\pi}$

**Output:** a set of selected variables

- 1: Rank the variables by their test statistics so that  $z_{(1)} > z_{(2)} > \dots > z_{(p)}$
- 2: Compute  $\hat{s} = \hat{\pi}p$
- 3: For  $j = 1, 2, \dots, p$ , compute

$$\widehat{FNP}(z_{(j)}) = \max\{1 - j/\hat{s} + (p - \hat{s})\bar{\Phi}(z_{(j)})/\hat{s}, 0\}$$

- 4: Let  $k = 1$
- 5: **while**  $\widehat{FNP}(z_{(k)}) \geq \beta$  **do**  $k = k + 1$
- 6: **end while**
- 5: Obtain variables ranked at  $1, \dots, k - 1$

---

## 5 Simulation

In this section, We compare the empirical performances of the new method (DCOE) with existing false negative control methods. Such methods are relatively limited and have only appeared recently. For example, the AFNC method in [Jeng et al. \(2016\)](#) was proposed to control the so-called signal missing rate to detect rare variants in genome-wide association study ([Jeng et al., 2016](#)); the MDR method in [Cai and Sun \(2017\)](#) was proposed to control the so-called missed discovery rate using an empirical Bayesian approach ([Cai and Sun, 2017](#)); the AdSMR method in [Jeng et al. \(2019\)](#) focuses on controlling a FNP-based exceedance probability; and the FNC-Reg approach in [Jeng and Chen \(2019b\)](#) considers FNP control in linear regression. Among these methods, AFCN, MDR, and FNC-Reg are more comparable to DCOE because they all require the input of a user-specified control level. However, AFNC and MDR were developed under the independent assumption, and FNC-Reg considered specific dependence and signal sparsity conditions to facilitate accurate precision matrix estimation and bias mitigation. All of these methods require estimates of the number of signals. For a fair comparison, we implement the same estimator  $\hat{s} = p \cdot \hat{\pi}$  to all the methods.

### 5.1 One-dimensional problems

In this section, we generate the test statistics by (13) with a covariance matrix that has 20 diagonal blocks with block sizes randomly generated from 10 to 100. The non-zero off-diagonal correlations are set at 0.5. The dependence parameter  $\eta$  varies from sample to sample due to the random block size. In the first set of examples, signal sparsity is fixed with  $\gamma = 0.3$ , and signal intensity (A) increases from 3 to 5. In the second set of examples, signal intensity is fixed and signal sparsity varies as  $\gamma = 0.3$  and 0.5.

The performances of the methods are evaluated by three measures. The first two measures, FNP and FDP are the same as in [Table 1](#). The last measure is the Fowlkes-Mallows index ([Fowlkes and Mallows, 1983](#); [Halkidi et al., 2001](#)), which summarizes the measures of

FNP and FDP by calculating the geometric mean of (1–FNP) and (1–FDP), i.e.,

$$\text{FM-index} = \sqrt{(1 - \text{FNP}) \times (1 - \text{FDP})}.$$

Higher values of the FM-index indicate better classification results. The FM-index is a sensible summary measure in high-dimensional settings with sparse alternative cases because the scale of its FDP component is more comparable to that of its FNP component than the classical false positive proportion (FPP = number of false positives/number of null cases). Because the methods compared in this section all focus on false negative control, it is appropriate to use FM-index to evaluate their relative efficiency.

Results of the first set of examples are summarized in [Table 2](#). First, because the estimation boundary  $\mu_{min}$  remains at 2.14 in these examples, the condition  $A_j - \mu_{min} \rightarrow \infty$  in [Theorem 2.2](#) is not well supported for smaller  $A_j$  ( $= A$  in these examples). Also, because the estimator  $\hat{s}$  underestimates the true  $s$  when signal intensity is not strong enough, DCOE implemented with  $\hat{s}$  selects less variables than actually needed to reach the nominal level of  $\beta$ . These result in inflated realized FNP as seen in [Table 2](#). Further, as  $A$  increases, the mean value of FNP of DCOE gets closer to the nominal level of  $\beta$ , which agrees with the claims in [\(17\)](#) and [\(18\)](#) in [Proposition 4.1](#). Among the three methods presented in [Table 2](#), DCOE shows a clear tendency to adapt to the nominal level of  $\beta$  as  $A$  increases, which is not observed for the other two methods. DCOE also has the lowest FNP values. In terms of the FM-index, DCOE generally outperforms the other two methods especially when signal intensity gets stronger.

The second set of examples have  $\gamma$  increased from 0.3 to 0.5, so that the number of signals deceases from 205 to 45. The nominal level of  $\beta$  also varies. The signal intensity  $A$  is fixed at 5. Results summarized in [Table 3](#) show that when signals get sparser with larger  $\gamma$ , the performances of all three methods deteriorate by including more noise variables. However, DCOE continues to outperform the other two methods in adapting to different nominal levels and incurring less false positives. Its advantage seems to be more prominent when signals get more sparse.

Table 2: Effect of signal intensity on different FN control methods with estimated  $s$ . Mean values and standard deviations (in brackets) of the realized FNP, FDP, and the FM-index are presented for the proposed DCOE method and two existing methods, AFNC and MDR from 100 replications.

		FNP	FDP	FM-index
$A = 3$	DCOE( $\beta = 0.1$ )	<b>0.28</b> (0.12)	0.13 (0.14)	<b>0.78</b> (0.04)
	AFNC( $\beta = 0.1$ )	0.19 (0.11)	0.22 (0.18)	0.78 (0.07)
	MDR( $\beta = 0.1$ )	0.09 (0.08)	0.49 (0.26)	0.65 (0.15)
$A = 4$	DCOE( $\beta = 0.1$ )	<b>0.16</b> (0.07)	0.06 (0.12)	<b>0.88</b> (0.05)
	AFNC( $\beta = 0.1$ )	0.07 (0.04)	0.14 (0.18)	0.89 (0.10)
	MDR( $\beta = 0.1$ )	0.06 (0.05)	0.37 (0.32)	0.74 (0.18)
$A = 5$	DCOE( $\beta = 0.1$ )	<b>0.10</b> (0.04)	0.04 (0.12)	<b>0.93</b> (0.06)
	AFNC( $\beta = 0.1$ )	0.01 (0.01)	0.36 (0.35)	0.75 (0.26)
	MDR( $\beta = 0.1$ )	0.04 (0.04)	0.36 (0.33)	0.75 (0.19)

Table 3: Effect of nominal level and signal sparsity on different FN control methods with estimated  $s$ . Same notations as in [Table 2](#) are used.

		FNP	FDP	FM-index
$\gamma = 0.3$	DCOE( $\beta = 0.1$ )	<b>0.10</b> (0.04)	0.04 (0.12)	<b>0.93</b> (0.06)
	AFNC( $\beta = 0.1$ )	0.01 (0.01)	0.36 (0.35)	0.75 (0.26)
	MDR( $\beta = 0.1$ )	0.04 (0.04)	0.36 (0.33)	0.75 (0.19)
	DCOE( $\beta = 0.2$ )	<b>0.19</b> (0.06)	0.02 (0.08)	<b>0.89</b> (0.03)
	AFNC( $\beta = 0.2$ )	0.01 (0.01)	0.21 (0.29)	0.86 (0.20)
	MDR( $\beta = 0.2$ )	0.08 (0.09)	0.26 (0.28)	0.80 (0.14)
	DCOE( $\beta = 0.1$ )	<b>0.09</b> (0.05)	0.15 (0.29)	<b>0.85</b> (0.18)
	AFNC( $\beta = 0.1$ )	0.00 (0.01)	0.73 (0.28)	0.44 (0.27)
	MDR( $\beta = 0.1$ )	0.03 (0.05)	0.56 (0.44)	0.54 (0.34)
$\gamma = 0.5$	DCOE( $\beta = 0.2$ )	<b>0.16</b> (0.09)	0.12 (0.27)	<b>0.83</b> (0.15)
	AFNC( $\beta = 0.2$ )	0.01 (0.02)	0.60 (0.36)	0.55 (0.31)
	MDR( $\beta = 0.2$ )	0.07 (0.10)	0.54 (0.45)	0.54 (0.32)

## 5.2 A Two-dimensional example

In this example, we simulate a  $100 \times 100$  two-dimensional grid graph with the signal region demonstrated in [Figure 4a](#). The signal region covers 994 nodes, i.e.  $s = 994$ . At each node, test statistic  $Z_{ij}$  is generated independently from  $N(A_{ij}, 1)$ , where  $A_{ij} \sim \text{Uniform}[1, 2.5]$  if  $(i, j)$  is in the signal region, and  $A_{ij} = 0$  otherwise.

We apply the proposed DCOE method with different nominal levels and compare the results with those of BH-FDR, AFNC, and MDR. [Figure 4b](#) shows the selected nodes of

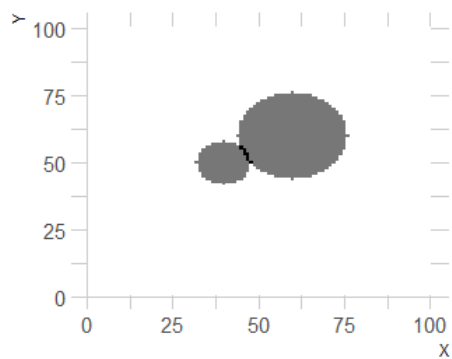
BH-FDR with  $\alpha = 0.05$  in a single trial, [Figure 4c](#) and [Figure 4d](#) show the results of AFNC and MDR with  $\beta = 0.1$ , respectively, and [Figure 4e](#) and [Figure 4f](#) show the results of DCOE with  $\beta = 0.1$  and  $0.5$ , respectively. It can be seen that DCOE identifies more true signals and delineates the signal region better than BH-FDR even when  $\beta$  is as large as  $0.5$ . On the other hand, it pays the price with some more false positives. Compared to AFNC and MDR, DCOE has less false positives and less true positives, which does not seem to impair its ability to delineate the signal region much.

## 6 Application

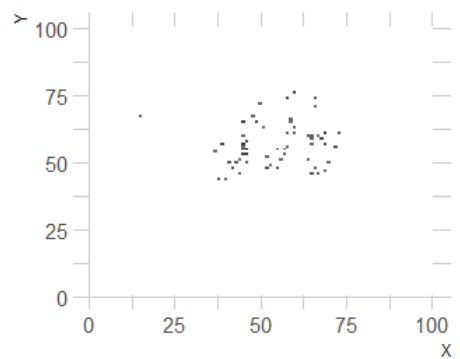
We obtained the fMRI data from the Individual Brain Charting (IBC) Project, which is a publicly available high-resolution fMRI dataset for cognitive mapping ([Pinho et al., 2018](#)). The dataset refers to a cohort of 12 participants performing different tasks, addressing both low- and high- level cognitive functions. We focus on the data from the saccade experiment for spatial cognition, in which ocular movements were performed according to the displacement of a fixation cross from the center toward peripheral locations in the image displayed.

The data were collected using a Gradient-Echo (GE) pulse, whole-brain Multi-Band (MB) accelerated Echo-Planar Imaging (EPI)  $T2^*$ -weighted sequence with Blood-Oxygenation-Level-Dependent (BOLD) contrasts, and preprocessed using *PyPreprocess*, a collection of python tools for preprocessing fMRI data. In order to assess the statistical significance of the differences among evoked BOLD responses, test statistics are computed at every voxel for each contrast using General Linear Model (GLM). All images are confined to an average mask of the gray matter across subjects, which yields 371,817 voxels at the chosen resolution. More details about the dataset can be found in [Pinho et al. \(2018\)](#).

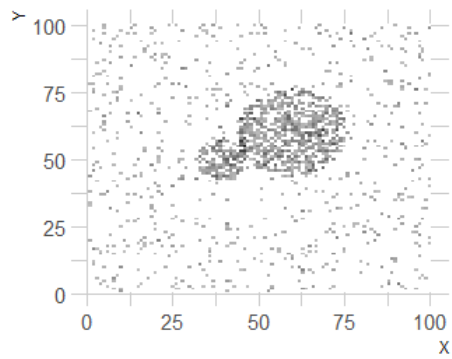
We apply the proposed method (DCOE), the popular BH-FDR procedure, and the existing AFNC and MDR methods to the statistical maps of 12 participants. The numbers of selected voxels for each participant are reported in [Table 4](#). Among all the methods, BH-FDR selects the least voxels and MDR selects the most voxels. DCOE selects more than BH-FDR and less than AFNC and MDR.



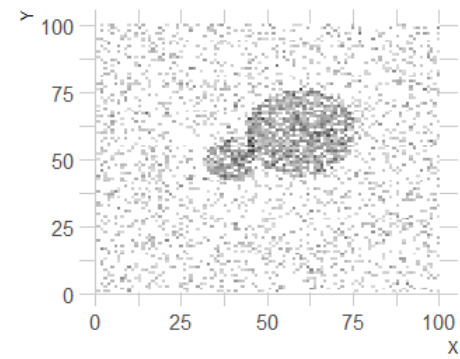
(a) Pure Signals



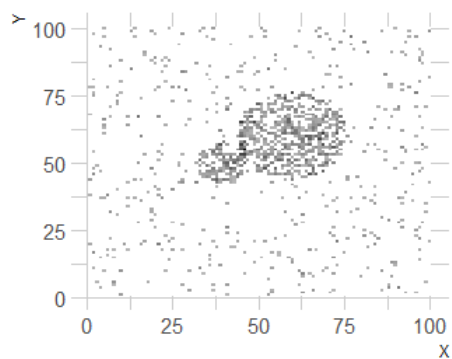
(b) BH-FDR( $\alpha = 0.05$ )



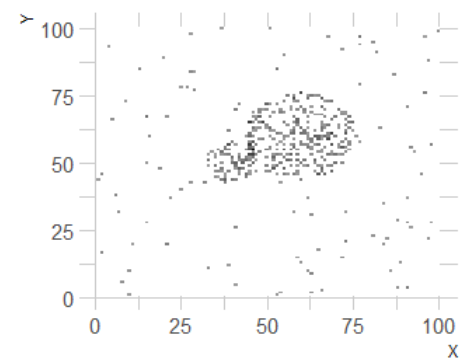
(c) AFNC( $\beta = 0.1$ )



(d) MDR( $\beta = 0.1$ )



(e) DCOE( $\beta = 0.1$ )



(f) DCOE( $\beta = 0.5$ )

Figure 4: Comparison results from a single trial. The clustered signals are shown in plot (a). Plots (b) - (f) demonstrate the results of different methods.

Table 4: Numbers of selected voxels by different methods.

Subject	BH-FDR( $\alpha = 0.05$ )	DCOE( $\beta = 0.1$ )	AFNC( $\beta = 0.1$ )	MDR( $\beta = 0.1$ )
sub-1	18500	19379	24837	27793
sub-2	44902	52614	70981	78288
sub-4	15291	31852	44893	60356
sub-5	8623	23236	37333	62976
sub-6	17778	29298	40537	47812
sub-7	25011	51405	76931	88407
sub-8	35463	47467	65238	74915
sub-9	20846	35662	50516	63989
sub-11	28586	32989	43147	48892
sub-12	20469	27388	36256	38353
sub-13	21365	44094	63192	74508
sub-14	21067	58494	85889	96651

Figure 5 illustrates the selected voxels of each method in the image of a single participant (sub-5) from posterior, superior, and left views. The figure is generated using the Multi-image Analysis GUI (<http://ric.uthscsa.edu/mango/>). We look into several regions that are known to be associated with saccadic eye movements. First, the visual cortex (VC) on occipital lobe in the posterior region of the brain, as indicated in Figure 5d, is the primary cortical region that receives, integrates, and processes visual information (Bodis-Wollner et al., 1997). We can see that all four methods have identified voxels in VC. However, the results of DCOE, AFNC and MDR seem to match the VC region much better than that of BH-FDR. From the superior and left views, it shows that BH-FDR has only a few or no discoveries in the frontal eye fields (FEF) located in Brodmann area 8, the supplementary eye fields (SEF) located in Broadmann area 6, and the posterior parietal cortex (PPC). The locations of FEF, SEF, and PPC are indicated in Figure 5e and Figure 5f. FEF and SEF are believed to play important roles in visual attention and eye movements as electrical stimulation of these areas evokes eye movements (Bruce and Goldberg, 1985; Bruce et al., 1985). PPC, on the other hand, is related to decision making and saccades (Goldberg et al., 2002; Schluppeck et al., 2005). It can be seen that DCOE, AFNC, and MDR have better power for identifying signal voxels in FEF, SEF, and PPC. Among these three methods, DCOE selects the least scattered or isolated voxels that are not functionally relevant to saccades.

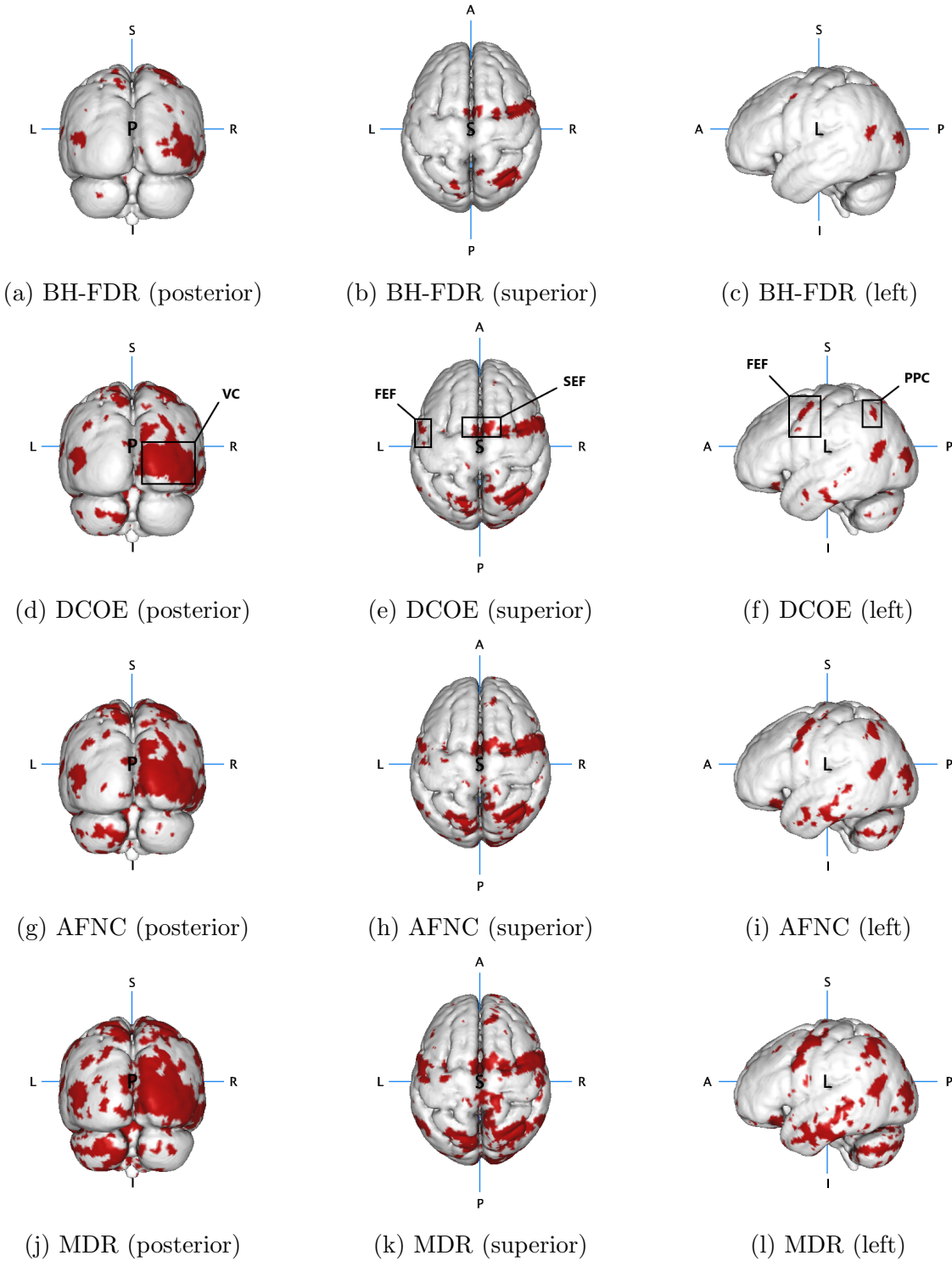


Figure 5: The selected voxels from BH-FDR, DCOE, AFNC, and MDR for a single participant (sub-05).

## 7 Conclusion and Discussion

In this paper, we develop a new analytic framework to perform inference on signals that are detectable yet unidentifiable. A new dual control method is proposed to control FNP at a user-specified level and, at the same time, regulate the unnecessary false positives to achieve the target FNP level. The new method is developed under arbitrary covariance dependence calibrated through a dependence parameter whose scale is compatible with the existing formulation in sparse inference. Utilizing the new calibration, we are able to explicate the joint effects of covariance dependence and signal sparsity and interpret the results using a phase diagram to gain important insight.

We demonstrate the finite sample performance of the dual control method in simulation and apply the method to identify functionally relevant regions for saccadic eye movement using fMRI data. Its results are compared with those of other methods and with regions that are known to be associated with saccade. The new method seems to benefit from its dual control property and exhibits a good balance in identifying signal voxels in the functionally relevant regions and avoiding the scattered noise voxels.

This new method will be useful in, for example, pre-surgical fMRI data analysis, where efficient false negative control is of vital importance because neurosurgical patients are likely to experience significant harm from mistakenly deeming a region to be functionally uninvolved and subsequently resecting critical tissues. In a broad sense, our study expands the frontier of high-dimensional sparse inference by bridging an important methodological gap.

## 8 Appendix

This section provides the proofs of [Theorem 2.1](#), [Theorem 2.2](#), and [Proposition 4.1](#), as well as additional simulation results. We will frequently use the following result on Mill's ratio:

$$\bar{\Phi}(x) \leq x^{-1}\phi(x) \quad \text{for any } x > 0.$$

The symbol  $C$  denotes a genetic, finite constant whose value can be different at different occurrences.

## 8.1 Proof of Theorem 2.1

For notation simplicity, let

$$B(t) = 1 - R(t)/s + (p - s)\bar{\Phi}(t)/s. \quad (19)$$

Then  $\widehat{FNP}(t) = \max\{B(t), 0\}$ , and it is sufficient to show that

$$|B(t) - FNP(t)| = o_p(1) \quad \text{when } B(t) \geq 0 \quad (20)$$

and

$$FNP(t) = o_p(1) \quad \text{when } B(t) < 0. \quad (21)$$

Consider (20) first. By the definitions of  $B(t)$  and  $FNP(t)$ ,

$$|B(t) - FNP(t)| = |s^{-1}(R(t) - (p - s)\bar{\Phi}(t)) - s^{-1}(R(t) - FP(t))| = s^{-1}|FP(t) - (p - s)\bar{\Phi}(t)|.$$

Therefore, it is sufficient to show

$$s^{-1}|FP(t) - (p - s)\bar{\Phi}(t)| = o_P(1). \quad (22)$$

Recall the definition of  $\mu_1$  and  $\mu_2$  in (8). The following proof is composed of two parts. The first part assumes  $t \geq \mu_1$  and the second part assumes  $\mu_2 \leq t < \mu_1$ .

Consider the first part. It's sufficient to show  $s^{-1}FP(t) = o_P(1)$  and  $s^{-1}(p - s)\bar{\Phi}(t) = o(1)$  with  $t \geq \mu_1$ . By Mill's ratio and the re-parameterization of  $s$  in  $\gamma$ ,

$$s^{-1}(p - s)\bar{\Phi}(t) \leq \frac{Cpe^{-t^2/2}}{ts} \leq \frac{C}{\sqrt{\log p}} = o(1).$$

On the other hand, for a fixed constant  $a > 0$ ,

$$P(s^{-1}\text{FP}(t) > a) \leq \frac{E(\text{FP}(t))}{as} \leq \frac{p \max_{j \in I_0} P(z_j > t)}{as} \leq \frac{Cp\bar{\Phi}(t)}{s} = o(1).$$

Therefore, the claim in (22) is justified for  $t \geq \mu_1 = \sqrt{2\gamma \log p}$ .

Next we present the second part of the proof with  $\mu_2 \leq t < \mu_1$ . Define

$$D_p = s^{-2}e^{-t^2/2}\|\Sigma\|_1 \log p.$$

By the condition  $t \geq \mu_2$  and the re-parameterizations of  $\|\Sigma\|_1$  in  $\eta$  and  $s$  in  $\gamma$ , it can be shown that

$$D_p = p^{2\gamma-\eta}e^{-t^2/2} \log p \leq \log^{-1} p = o(1).$$

Then, (22) is implied by

$$s^{-1}|\text{FP}(t) - (p-s)\bar{\Phi}(t)| = o_P(\sqrt{D_p}). \quad (23)$$

Apply Chebyshev's inequality,

$$P(s^{-1}|\text{FP}(t) - (p-s)\bar{\Phi}(t)| > \sqrt{D_p}) \leq \frac{Var(\text{FP}(t))}{s^2 D_p}. \quad (24)$$

We have the following lemma for the order of  $Var(\text{FP}(t))$  under dependence. The proof is essentially the same as that of Lemma 5.2 in [Jeng \(2021\)](#). We omit the details to save space.

**Lemma 8.1.** *Consider model (6). Denote  $\Sigma_0$  as the correlation matrix of  $Z_j, j \in I_0$ . We have*

$$Var\left(\sum_{j \in I_0} 1_{\{z_j > t\}}\right) = O(e^{-t^2/2}\|\Sigma_0\|_1).$$

Therefore,  $Var(\text{FP}(t)) = Var(\sum_{j \in I_0} 1_{\{z_j > t\}}) \leq Ce^{-t^2/2}\|\Sigma_0\|_1 \leq Ce^{-t^2/2}\|\Sigma\|_1$ , and it follows that

$$\frac{Var(\text{FP}(t))}{s^2 D_p} = o(1) \quad (25)$$

by the definition of  $D_p$ . Combining (24) and (25) gives (23), which justifies the claim in (22) for  $\mu_2 \leq t < \mu_1$ .

Finally, consider (21). It can be shown that  $B(t) < 0$  implies  $1 - \text{FP}(t)/s - \text{TP}(t)/s + (p - s)\bar{\Phi}(t)/s < 0$ , which, combined with  $\text{FNP}(t) = 1 - \text{TP}(t)/s$ , further implies

$$\text{FNP}(t) < s^{-1}(\text{FP}(t) - (p - s)\bar{\Phi}(t)).$$

Since the order of the right hand side has been derived in (22), (21) follows.  $\square$

## 8.2 Proof of Theorem 2.2

First, by Markov's inequality, for a fixed constant  $a > 0$ ,

$$\begin{aligned} P(\text{FNP}(\mu_{min}) > a) &= P(s^{-1} \sum_{j \in I_1} 1_{\{z_j \leq \mu_{min}\}} > a) \leq \frac{1}{as} \sum_{j \in I_1} P(Z_j \leq \mu_{min}) \\ &\leq \frac{1}{a} \max_{j \in I_1} P(N(0, 1) \leq \mu_{min} - A_j) = o(1), \end{aligned}$$

where the last step is by the condition on  $A_j$ . Therefore,  $\text{FNP}(\mu_{min}) = o_P(1)$ . By Theorem 2.1, we have  $|\widehat{\text{FNP}}(\mu_{min}) - \text{FNP}(\mu_{min})| = o_P(1)$ , which implies  $\widehat{\text{FNP}}(\mu_{min}) = o_P(1)$ . Then, by the construction of  $\hat{t}(\beta)$ , we have  $P(\hat{t}(\beta) \geq \mu_{min}) \rightarrow 1$ . Consequently, since  $\hat{t}(\beta)$  is random,

$$\begin{aligned} &\lim_{p \rightarrow \infty} P(|\widehat{\text{FNP}}(\hat{t}(\beta)) - \text{FNP}(\hat{t}(\beta))| > a) \\ &= \lim_{p \rightarrow \infty} E \left[ E \left( 1 \{ |\widehat{\text{FNP}}(\hat{t}(\beta)) - \text{FNP}(\hat{t}(\beta))| > a \} | \hat{t}(\beta) \right) \right] \\ &= E \left[ \lim_{p \rightarrow \infty} E \left( 1 \{ |\widehat{\text{FNP}}(\hat{t}(\beta)) - \text{FNP}(\hat{t}(\beta))| > a \} | \hat{t}(\beta) \right) \right] = 0, \end{aligned}$$

where the second step above is by dominated convergence theorem and the last step is by Theorem 2.1. Therefore,  $|\widehat{\text{FNP}}(\hat{t}(\beta)) - \text{FNP}(\hat{t}(\beta))| = o_P(1)$ . Now, since  $\widehat{\text{FNP}}(\hat{t}(\beta)) < \beta$  almost surely by the construction of  $\hat{t}(\beta)$ , claim in (11) follows.

Next, let's consider the claim in (12). Because  $\tilde{t} > \hat{t}(\beta)$ , the construction of  $\hat{t}(\beta)$  implies that  $\widehat{\text{FNP}}(\tilde{t}) \geq \beta$  almost surely. On the other hand, because  $\tilde{t} > \hat{t}(\beta) \geq \mu_{min}$  with probability tending to 1, similar arguments as the above lead to  $|\widehat{\text{FNP}}(\tilde{t}) - \text{FNP}(\tilde{t})| = o_P(1)$ . Therefore, the claim in (12) follows.  $\square$

### 8.3 Proof of Proposition 4.1

The consistency of  $\hat{\pi}^*$  is based on the following two lemmas, which are implied by Theorem 2.2 and 2.3 in [Jeng \(2021\)](#).

**Lemma 8.2.** *Consider model (6). Let  $\delta(t) = [\bar{\Phi}(t)]^{1/2}$ . Then, there exists a bounding sequence  $c_{p,\delta}^* = O(\sqrt{\bar{\rho} \cdot \log p})$ , and the corresponding estimator  $\hat{\pi}_\delta^*$  satisfies  $P(\hat{\pi}_\delta^* < \pi) \rightarrow 1$ . Moreover, for  $\pi$  satisfying  $0 < \pi \ll 1$ , if  $\tau = \min_{j \in I_1} A_j \gg 1$  and*

$$\tau - \bar{\Phi}^{-1} \left( \frac{\pi^2}{\bar{\rho} \cdot \log p} \right) \rightarrow \infty, \quad (26)$$

*then  $P(\hat{\pi}_\delta^* > (1 - \epsilon)\pi) \rightarrow 1$  for any constant  $\epsilon > 0$ .*

**Lemma 8.3.** *Consider model (6). Let  $\delta(t) = \bar{\Phi}(t)$ . Then, there exists a bounding sequence  $c_{p,\delta}^* = O(\sqrt{\log p})$ , and the corresponding estimator  $\hat{\pi}_\delta^*$  satisfies  $P(\hat{\pi}_\delta^* < \pi) \rightarrow 1$ . Moreover, for  $\pi$  satisfying  $0 < \pi \ll 1$ , if  $\tau = \min_{j \in I_1} A_j \gg 1$  and*

$$\tau - \bar{\Phi}^{-1} \left( \frac{\pi}{\sqrt{\log p}} \right) \rightarrow \infty. \quad (27)$$

*then  $P(\hat{\pi}_\delta^* > (1 - \epsilon)\pi) \rightarrow 1$  for any constant  $\epsilon > 0$ .*

Recall that  $\pi = p^{-\gamma}$ ,  $\gamma \in (0, 1]$ , and  $\bar{\rho} = p^{-\eta}$ ,  $\eta \in [0, 1]$ . Recall  $\mu_1$  and  $\mu_2$  in (8). Direct calculation shows that when  $\tau - \mu_2 \rightarrow \infty$ , the condition in (26) is satisfied, and when  $\tau - \mu_1 \rightarrow \infty$ , the condition in (27) is satisfied. Therefore, given  $\tau = \min_{j \in I_1} A_j - \mu_{min} \rightarrow \infty$ , the consistency of the estimator  $\hat{\pi}^* = \max\{\hat{\pi}_{0.5}, \hat{\pi}_1\}$  holds as in (16).

Next consider the claims in (17) and (18). Similar arguments as in the proof of [Theorem 2.2](#) can be applied, and we only need to show that [Theorem 2.1](#) continues to hold with

$\widehat{\text{FNP}}(t)$  replaced by  $\widehat{\text{FNP}}_{\hat{s}}(t)$ . Given the result in (9), it is sufficient to show  $|\widehat{\text{FNP}}_{\hat{s}}(t) - \widehat{\text{FNP}}(t)| = o_P(1)$  for  $t \geq \mu_{min}$ , which is implied by

$$|B_{\hat{s}}(t) - B(t)| = o_P(1) \quad \text{for } t \geq \mu_{min}, \quad (28)$$

given the definition of  $B(t)$  in (19). By direct calculation,

$$\begin{aligned} |B_{\hat{s}}(t) - B(t)| &= |(\hat{s}^{-1} - s^{-1})(\text{R}(t) - p\bar{\Phi}(t))| \\ &\leq |\hat{s}^{-1} - s^{-1}| \cdot \text{TP}(t) + |\hat{s}^{-1} - s^{-1}| \cdot |\text{FP}(t) - p\bar{\Phi}(t)|. \end{aligned} \quad (29)$$

Given  $P((1 - \delta) < \hat{s}/s < 1) \rightarrow 1$  for any  $\delta > 0$ , it can be shown that

$$P(|\hat{s}^{-1} - s^{-1}| < \frac{\delta}{1 - \delta} s^{-1}) \rightarrow 1.$$

On the other hand,  $\text{TP}(t) \leq s$  almost surely. Then it follows that the first term in (29),

$$|\hat{s}^{-1} - s^{-1}| \cdot \text{TP}(t) = o_p(1).$$

For the second term in (29),

$$|\hat{s}^{-1} - s^{-1}| \cdot |\text{FP}(t) - p\bar{\Phi}(t)| < \frac{\delta}{1 - \delta} s^{-1} |\text{FP}(t) - p\bar{\Phi}(t)| \leq \frac{\delta}{1 - \delta} (s^{-1} |\text{FP}(t) - (p - s)\bar{\Phi}(t)| + \bar{\Phi}(t))$$

with probability tending 1, where  $\bar{\Phi}(t) = o(1)$  for  $t \geq \mu_{min}$ , and it has been shown as for (22) that  $s^{-1} |\text{FP}(t) - (p - s)\bar{\Phi}(t)| = o_P(1)$  for  $t \geq \mu_{min}$ . Then it follows that

$$|\hat{s}^{-1} - s^{-1}| \cdot |\text{FP}(t) - p\bar{\Phi}(t)| = o_P(1).$$

Summing up the above gives (28).  $\square$

## References

Arias-Castro, E., E. J. Candès, and Y. Plan (2011). Global testing under sparse alternatives: Anova, multiple comparisons and the higher criticism. *The Annals of Statistics* 39(5), 2533–2556.

Barber, R. F. and E. J. Candès (2015). Controlling the false discovery rate via knockoffs. *Ann. Statist.* 43(5), 2055–2085.

Benjamini, Y. and Y. Hochberg (1995). Controlling the false discovery rate: a practical and powerful approach to multiple testing. *J. R. Statist. Soc. Ser. B* 57(1), 289–300.

Bodis-Wollner, I., S. Bucher, K. Seelos, W. Paulus, M. Reiser, and W. Oertel (1997). Functional mri mapping of occipital and frontal cortical activity during voluntary and imagined saccades. *Neurology* 49(2), 416–420.

Bruce, C. J. and M. E. Goldberg (1985). Primate frontal eye fields. i. single neurons discharging before saccades. *Journal of neurophysiology* 53(3), 603–635.

Bruce, C. J., M. E. Goldberg, M. C. Bushnell, and G. B. Stanton (1985). Primate frontal eye fields. ii. physiological and anatomical correlates of electrically evoked eye movements. *Journal of neurophysiology* 54(3), 714–734.

Cai, T., J. Jin, and M. Low (2007). Estimation and confidence sets for sparse normal mixtures. *The Annals of Statistics* 35(6), 2421–2449.

Cai, T. T., X. J. Jeng, and J. Jin (2011). Optimal detection of heterogeneous and heteroscedastic mixtures. *Journal of the Royal Statistical Society: Series B (Statistical Methodology)* 73(5), 629–662.

Cai, T. T. and J. Jin (2010). Optimal rates of convergence for estimating the null density and proportion of nonnull effects in large-scale multiple testing. *The Annals of Statistics*, 100–145.

Cai, T. T. and W. Sun (2017). Optimal screening and discovery of sparse signals with applications to multistage high-throughput studies. *Journal of the Royal Statistical Society: Series B* 79(1), 197–223.

Candes, E., Y. Fan, L. Janson, and J. Lv (2018). Panning for gold: Model-x knockoffs for high dimensional controlled variable selection. *J. R. Statist. Soc. Ser. B* 80(3), 551–577.

Donoho, D. and J. Jin (2004). Higher criticism for detecting sparse heterogeneous mixtures. *The Annals of Statistics* 32(3), 962–994.

Donoho, D. and J. Jin (2015). Special invited paper: Higher criticism for large-scale inference, especially for rare and weak effects. *Statistical Science*, 1–25.

Dudoit, S. and M. J. Van Der Laan (2007). *Multiple testing procedures with applications to genomics*. Springer Science & Business Media.

Fan, J., X. Han, and W. Gu (2012). Estimating false discovery proportion under arbitrary covariance dependence. *J. Amer. Statist. Assoc.* 107(499), 1019–1035.

Fowlkes, E. B. and C. L. Mallows (1983). A method for comparing two hierarchical clusterings. *Journal of the American statistical association* 78(383), 553–569.

Genovese, C. and L. Wasserman (2004). A stochastic process approach to false discovery control. *Annals of Statistics* 32, 1035–1061.

Goldberg, M. E., J. Bisley, K. D. Powell, J. Gottlieb, and M. Kusunoki (2002). The role of the lateral intraparietal area of the monkey in the generation of saccades and visuospatial attention. *Annals of the New York Academy of Sciences* 956(1), 205–215.

Halkidi, M., Y. Batistakis, and M. Vazirgiannis (2001). On clustering validation techniques. *Journal of intelligent information systems* 17(2-3), 107–145.

Jeng, X. J. (2021). Estimating the proportion of signal variables under arbitrary covariance dependence. *arXiv preprint arXiv:2102.09053*.

Jeng, X. J. and X. Chen (2019a). Predictor ranking and false discovery proportion control in high-dimensional regression. *J. Multivariate Anal.* 171, 163–175.

Jeng, X. J. and X. Chen (2019b). Variable selection via adaptive false negative control in linear regression. *Electron. J. Statist.* 13(2), 5306–5333.

Jeng, X. J., Z. J. Daye, W. Lu, and J.-Y. Tzeng (2016). Rare variants association analysis in large-scale sequencing studies at the single locus level. *PLoS computational biology* 12(6).

Jeng, X. J., T. Zhang, and J.-Y. Tzeng (2019). Efficient signal inclusion with genomic applications. *Journal of the American Statistical Association* 114, 1787–1799.

Meinshausen, N. and P. Bühlmann (2005). Lower bounds for the number of false null hypotheses for multiple testing of associations under general dependence structures. *Biometrika* 92(4), 893–907.

Meinshausen, N. and J. Rice (2006). Estimating the proportion of false null hypotheses among a large number of independently tested hypotheses. *Ann. Statist.* 34(1), 373–393.

Petticrew, M., A. Sowden, D. Lister-Sharp, and K. Wright (2000). False-negative results in screening programmes: systematic review of impact and implications. *Health technology assessment (Winchester, England)* 4(5), 1–120.

Pinho, A. L., A. Amadon, T. Ruest, M. Fabre, E. Dohmatob, I. Denghien, C. Ginisty, S. Becuwe-Desmidt, S. Roger, L. Laurier, et al. (2018). Individual brain charting, a high-resolution fmri dataset for cognitive mapping. *Scientific data* 5, 180105.

Schluppeck, D., P. Glimcher, and D. J. Heeger (2005). Topographic organization for delayed saccades in human posterior parietal cortex. *Journal of neurophysiology* 94(2), 1372–1384.